New Technologies for Monitoring the Precision Alignment of Large Detector Systems

Joseph A. Paradiso
Massachusetts Institute of Technology, Cambridge, MA 02139

joep@media.mit.edu

October, 1996

ABSTRACT

Two classes of inexpensive systems are described for performing dynamic, high-resolution measurements of the mechanical alignment between components of a large collider detector. One is a three-point optical system based on video cameras and simple frame processing, while the other is a multipoint stretched wire with 3-dimensional displacement readout. Test results are presented for both types of devices, and an application is outlined for a large muon system.

1) Introduction

Because of the small sagittas produced by very high-energy charged particles traversing the magnetic field of a detector system, errors in the mechanical alignment of the detector components can significantly degrade the precision of a reconstructed momentum measurement. Nowhere is this problem more acute than in large muon systems [1], where, in order to meet their stated momentum resolutions, proposed [2,3,4] detectors have required that alignment accuracies on the order of tens of microns are maintained between drift chamber packages often placed more than 10 meters apart. Rather than mounting the chambers precisely and requiring a muon system support structure to hold this level of accuracy, most proposed detector systems mandate that the alignment is periodically monitored, and the resulting measurements used to update the muon chamber positions during track reconstruction. While the muon tracks themselves can provide such an alignment reference as they traverse the entire detector [5], effects such as settling, thermal shift, and stresses coupled from the magnet system generally deform the support structure and move the muon detectors significantly over the intervals needed to collect sufficient muon statistics. For this reason, the designs of most large, precision muon detectors

Published in Nuclear Instruments and Methods in Physics Research, Sec. A (386), 1997

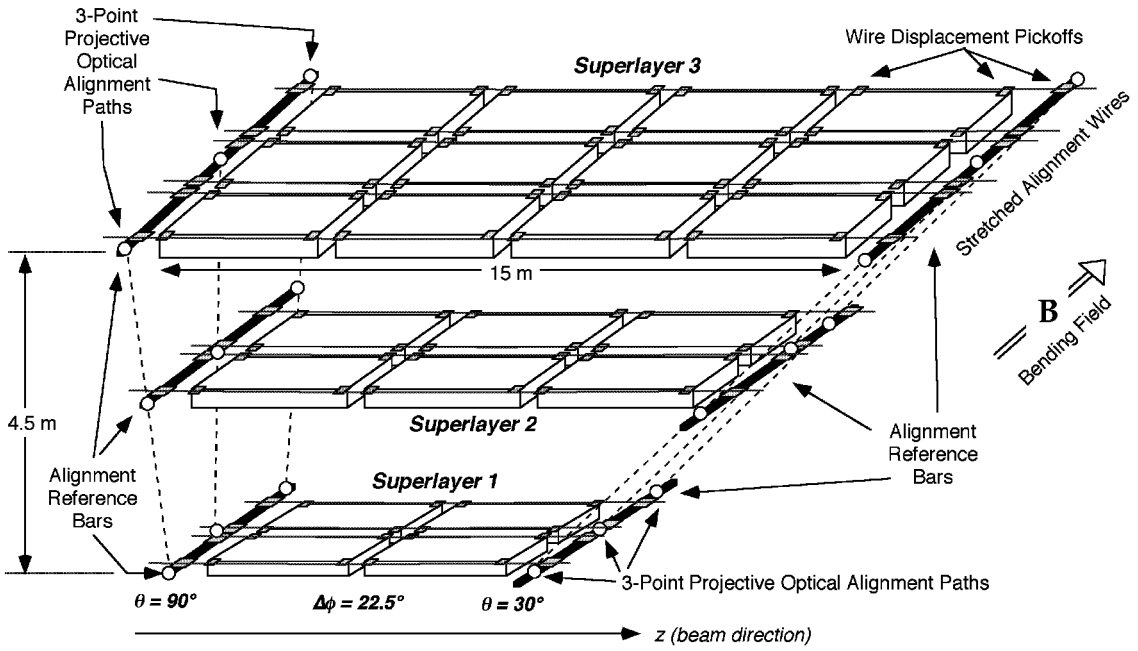

Figure 1: Schematic illustrating a hybrid axial/projective alignment scheme, as implemented for a module of the proposed GEM muon barrel.

include the specification of additional sensor systems to explicitly monitor the dynamic detector alignment.

An example of such a system is given in Figure 1, which shows a simplified schematic (omitting chamber tilts, overlaps, etc.) of a barrel module from the GEM muon detector [3], as proposed at the former SSC Laboratory. Under this design, high p_t muon tracks were measured at three superlayers in a 0.8 Tesla solenoidal field. In order to retain the desired precision at high momentum (i.e., $\Delta p_t/p_t \approx 5\%$ for the barrel detector at $p_t = 500$ GeV/c), this muon system must determine the net 3-point sagitta of a muon track to $\sigma = 55$ μm in the bending plane, as depicted in Fig. 1. After accounting [3] for the expected chamber resolution, mechanical tolerances, and multiple scattering, an error of $\sigma = 25$ μm was allotted to the determination of superlayer alignment, as projected onto the sagitta (bending) coordinate.

As seen in Figure 1, the large size of this system, together with the decision to use cathode strip chambers as muon detectors, mandated that muon superlayers were composed of multiple, tiled chamber packages. In addition to determining the alignment of the three composite superlayers, the positions of these discrete chamber packages must be accurately measured within each superlayer. Figure 1 solves this problem with an "axial/projective" geometry [6,7] that uses two types of alignment systems; an axial multipoint scheme that measures the position of chambers within each superlayer, and another 3-point projective

system to monitor the inter-superlayer positioning. The axial alignment systems transfer the superlayer alignment references to the barrel edges, thereby removing the need to place projective monitors inside the barrel at intermediate θ, which leads to large acceptance losses, among other difficulties [3,7].

This paper describes the technologies that were developed for realizing the projective and axial alignment measurements required by this approach. A set of stretched wires is used in each superlayer to define straight "axial" lines across the separate muon chamber packages stacked along the beam direction, and 3-point optical straight-line monitors are used to measure the "projective" sagitta error between the three superlayers at the barrel perimeters. A linear/quadratic interpolation algorithm [8] combines these measurements to compensate the misalignment errors occurring at muon track positions throughout the module.

Both axial and projective monitors are referenced to precision, stress-free, composite transfer plates ("Alignment Reference Bars" in Fig. 1), which thereby provide a common interface between the projective and axial alignment systems. Simulations [8,9,10] have indicated that the 25 μm sagitta alignment measurement goal can be obtained with 3-point projective monitors that resolve sagitta displacement to within $\sigma = 15$ μm (across optical paths reaching 9 meters), and stretched wires (up to 15 meters long) that resolve sagitta displacement to within $\sigma = 10$ μm, radial shifts (away from the beamline) to within $\sigma = 200$ μm, and axial positioning (along the beamline) of order 1 mm. In order to accommodate rapid assembly and potential structural drift, these monitors must operate over a dynamic range of 1 cm or more.

2) Wide-Range Optical Straightness Monitors

Three-point optical straightness monitors were first developed at the Draper Laboratory [11] for the L3 muon detector at LEP, where they were deployed as the RASNIK [12] system. These are simple devices composed of a light source, lens, and position-sensitive photodetector, as shown in Fig. 2. An image of a smooth-aperture, collimated source (i.e., LED) is projected onto a planar detector (i.e., quadrant photodiode) through a focusing lens. Displacements of the lens from the line between source and detector are measured as a shift in the illumination centroid at the photodiode. When precisely mounting one component (LED, lens, detector) at each superlayer, an array of these devices can dynamically monitor the 3-point interlayer sagitta error, as diagrammed in Fig. 1.

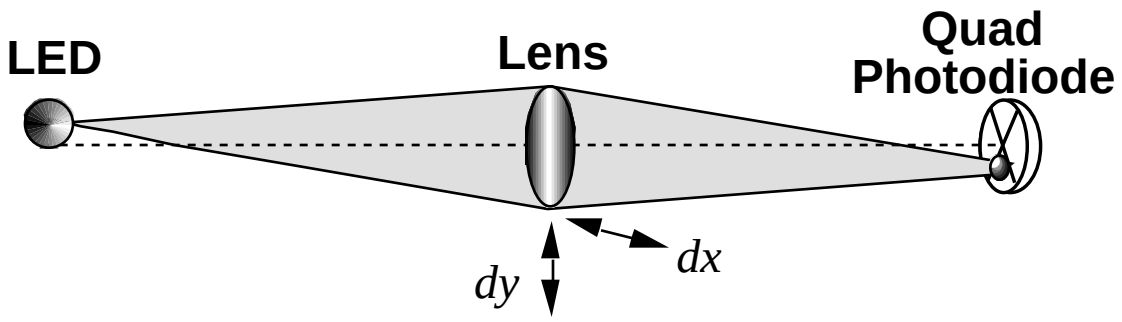

Figure 2: Standard 3-point straightness monitor as developed for the L3 muon detector.

With the lens at the midpoint, these devices have an implicit gain of two in the sagitta measurement; the offset read at the detector is twice the 3-point sagitta error. The measured displacement is relatively insensitive to rotations of the lens and LED (provided it exhibits a symmetric illumination profile) about their optical axes. The LED is modulated by a low-frequency carrier, and synchronously sampled [12,13] to effectively place a very narrow filter around the transmit frequency, minimizing the effects of any ambient light background, and enabling this device to be sensitive across very long optical paths.

Although simple LED/Lens/Quad-cell systems, such as depicted in Fig. 2, are proven to provide high accuracy in deployed detector systems (i.e., below 5 μm [12,14]) at minimal cost, their useful measurement range doesn't generally extend beyond 1-2 mm. The range of these alignment systems may be increased by replacing the quad-cell with a continuous lateral-effect photodiode [15,16] or by employing a wide-area diffuser over the LED and using a larger quadrant diode [17]. Another possibility [18] is to use a dense array of multiple LED's with overlapping linear range as measured at the quad cell, and illuminate each in succession. These techniques, however, can appreciably increase the hardware complication and expense, plus potentially degrade the alignment resolution beyond the 15 μm goal expressed in the previous section.

An early effort [19] in aligning muon chambers focused a single narrow light spot onto a 256-pixel CCD line array, and determined the offset of this feature relative to the sensor by taking the illumination centroid. Because only one feature is detected and a 1D sensor is used, this technique possessed certain drawbacks; the available range is still restricted to the active detector area, the measured position can be sensitive to ambient light (thus skewing the centroid), and only one axis of displacement is measured.

In the years since L3 was installed, dramatic progress has occurred in video technology and image processing. These advances have been exploited to evolve the simple straightness monitor of Fig. 2 into the Video Straightness Monitor (VSM) [20] or

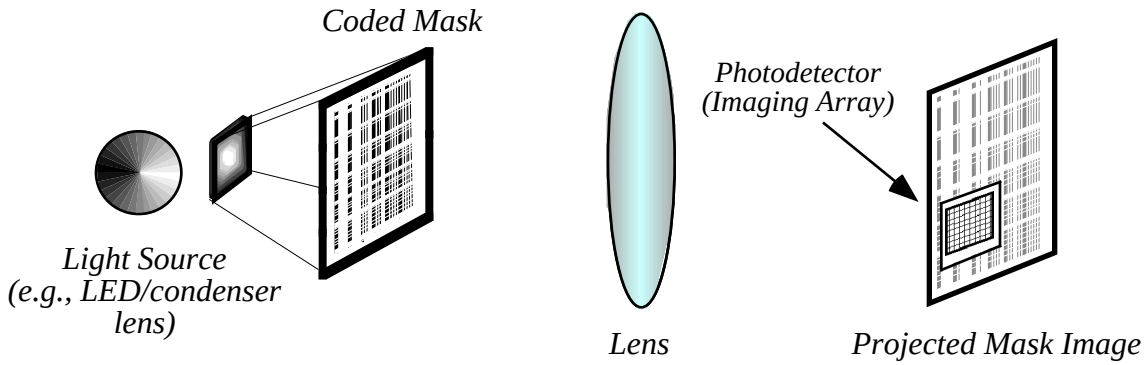

Figure 3: Video straightness monitor (VSM) scheme.

Video-RASNIK [21] of Fig. 3. Here, instead of putting a quadrant photodiode at the focal plane, an imaging array is placed there to collect much more information (i.e., tens of thousands of pixels, as opposed to only four). Likewise, instead of imaging a simple spot, as in Ref. [19] and Fig. 2, a complicated pattern is projected.

This approach has two major advantages. First, since the image is projected and detected over a full frame with many pixels, there is much more tolerance to local defects in the projected image and the focal plane array (this relieves much of the tedious calibration and component selection needed in RASNIK systems). Second, the operating range is greatly increased. Only a portion of the projected image need be seen by the sensitive array; if it is unambiguous, a correlation with the mask template will determine the offset between the array and the global image.

Recent advances in imaging technology and related microelectronics have dramatically reduced the cost and size of solid-state video cameras. Highly integrated, miniature monochrome cameras are now available, costing below $100 (US) in moderate quantities. Security and digital media applications drive much of this market, and a wide variety of such devices is now available [22]. They are self-contained, in that they typically require only 7-16 V of power and will output composite RS-170 video onto a 75 Ω cable. Several of these devices have been tested [23] for VSM application. Two that were successfully used are shown in Fig. 4, both compared in size to a US quarter. At left is the CX-103 from Chinon Corporation, which features a $^1/_3$" multiplexed MOS photodiode array of 324 x 246 elements, dynamic exposure compensation, RS-170 video formatting, and sensitivity down to 2 Lux @ F1.8. A subsequent device, the CX-060, is even 50% smaller in area, features a 512 x 496 CCD array, and is sensitive to 0.5 Lux at F1.8. These units, however, still have discrete IC's to clock the CCD and process the video. At right, in contrast, is the "Peach" video camera [24] from VVL corporation in Edinburgh,

Figure 4: Two of the small, inexpensive, monochrome video cameras tested for VSM application; the CX-103 (left) and VVL Peach (right).

Scotland, which has the sensor ($^1/_2$" array of 312 x 287 photodiode pixels operating down to 5 Lux @ F1.8) plus all CCIR video formatting and signal processing integrated onto the same CMOS monolithic. This technology has an exploding future in many emerging commercial applications [25], and is still being aggressively developed; inexpensive devices are now available [26,27] that send digital data directly from the video array and/or on-chip frame buffers.

In order to be useful for detector alignment, these devices must often perform in a strong magnetic field. Some of these small cameras have been seen to fail at fields beyond 1 KG, generally because of inductive elements used in the circuitry. Others, however, such as the Supercircuits PC-18XS, have been successfully used in fields of up to 1.5 Tesla to observe patients in magnetic resonance imagers [28]; with simple modification, the VVL Peach has likewise been used in high-field MRI environments.

In some detector applications, the cameras are required to tolerate significant radiation dose, although this is a lesser problem for a barrel muon system such as depicted in Fig. 1, where the cameras are far from the interaction point and well-shielded. Conventional CCD cameras are known to be somewhat sensitive to radiation damage because of the way in which the image charge is shifted across the chip in analog transport registers. Although radiation-hard CCD's have been developed for military and other applications [29], there are other, less expensive alternatives that can be used in environments with significant radiation exposure. Cameras based on photodiode arrays, such as the VVL Peach, address each pixel through an analog multiplexing scheme, thus are less sensitive to radiation. Tests [30] have indicated that the Peach is sufficiently radiation-hard for many alignment applications in detectors at high-luminosity colliders, such as the CERN LHC. In higher-dose environments, commercially-manufactured,

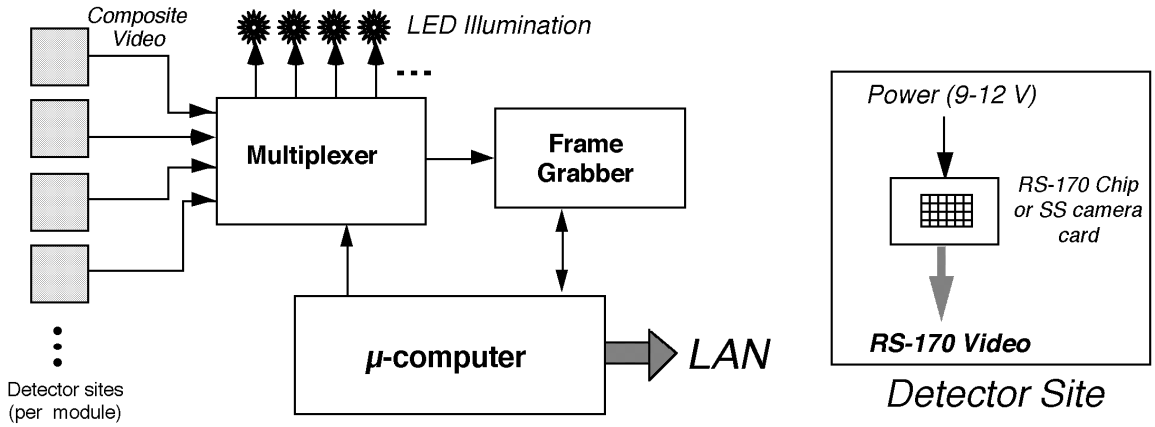

Figure 5: Data acquisition in a multiple-VSM system.

rad-hard Charge Injection Devices (CID's) can be used as the imaging arrays, since they tolerate much more radiation exposure (i.e., circa 10^6 rad and 10^{14} neutrons/cm^2) [31] .

As depicted in Fig. 5, the implementation of such a system in a large muon detector is very simple, potentially even more straightforward than deploying a system of standard RASNIK devices. All video outputs in a segment of the detector are routed to a multiplexer [32]; provided the cameras can also be powered through the video coax, only one cable is needed per camera site. When acquiring data, the supervisory processor addresses the multiplexer for the appropriate camera and activates the corresponding LED illuminator. Granted, the ability to easily do synchronous detection is lost here, but the multiplicity of projected features greatly reduces the sensitivity of the alignment measurement to background light. As shown in tests [18], the mask is well illuminated when using a combination of LED and condenser lens (which concentrates and directs the light like a flashlight beam), with a short (i.e., 10 cm) tube placed around the imaging array to mildly exclude extraneous light. Since these monochrome cameras are generally very responsive to the near infra-red, using an IR source and placing a matching IR filter over the camera can provide nearly complete attenuation of background light.

A series of frames is acquired at each camera site and averaged to attenuate transient thermal disturbance (tests in the laboratory [18] have indicated that averaging frames at 1 Hz for 15 seconds is normally sufficient), whereupon a simple correlation analysis fits the detected mask offset to its generated template, producing the required alignment measurements.

Because of jitter in their phase-lock loop circuitry, standard asynchronous consumer-quality frame grabbers are typically able to resolve no better than 20% of the pixel pitch [33] after they warm up, thus producing under 4 microns of error with a typical

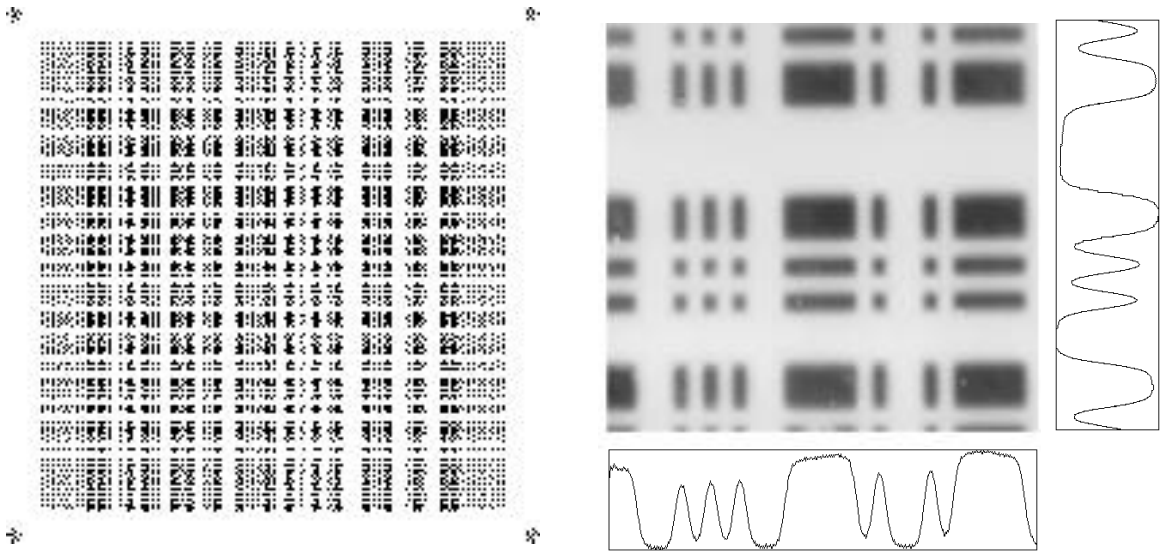

Figure 6: 2-Dimensional coincident barcode mask (left) and captured VSM frame (right).

imaging array, which is adequate for most detector alignment applications. Synchronous grabbers (with one memory location per pixel) are accurate to better than 3% of the pixel pitch [33], but such precision is generally not required here, sparing their additional expense and hardware complication.

The VSM image processing requirements are minimal when using an efficient mask coding and analysis procedure. Fig. 6 (left) shows the mask that was used for prototype tests; it is a coincident 2-dimensional barcode (with vertical bars running black-on-white, and horizontal bars running white-on-black), and was defined entirely in PostScript, then printed on a 1200 DPI Linotype and reduced to a square 2.4 cm on a side. A $^1/_3$" array thus sees 6% of the mask area (assuming a 1:1 projection); the barcode is designed such that at least one full digit (sandwiched between thick bars) can always be read anywhere in this field, disambiguating the camera offset in the projected image. In this scheme, the thick bars denote the beginning of a digit and the placement and presence of the narrow bars determine the digit's value; there are 18 separate "digits" across the entire mask.

An actual frame is displayed at right in Fig. 6, as captured in the VSM prototype across an 8 meter baseline with a ø = 42 mm lens at midpoint. The barcode can be well discerned; the small bars are 120 µm thick. The plots at bottom and right of this frame show horizontal (x) and vertical (y) projections (i.e., all pixels are summed into one row and one column), in which a segment of the x and y barcodes can be clearly seen.

An analysis program has been written to process the x and y projections of frame data. Fig. 7 shows a typical frame projection plot, annotated to describe the process.

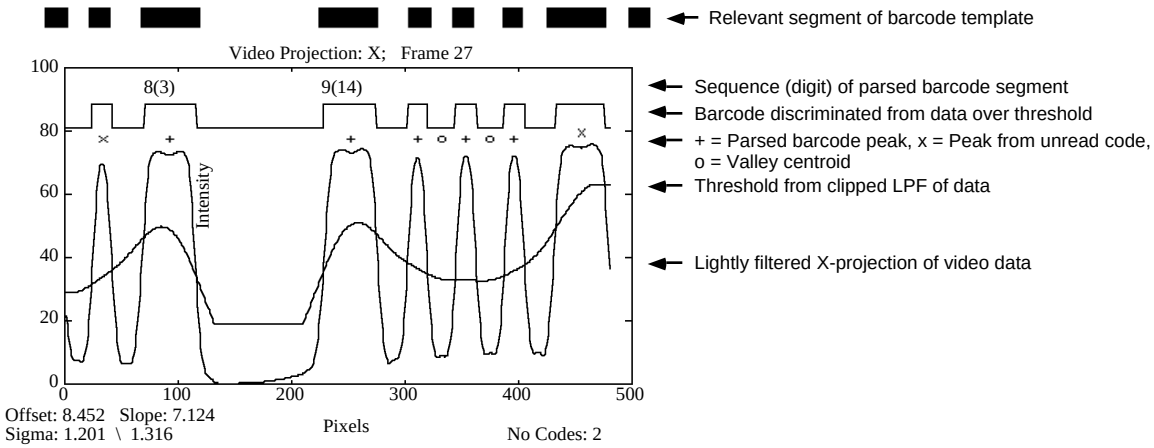

Figure 7: Analysis of the x-projection from a captured frame.

First, the projection data is slightly low pass filtered (to remove noise) and lightly high pass filtered (to attenuate baseline shifts), then discriminated by a floating threshold, recovering the barcode. Phase-invariant filters are used to avoid offset shifts. This code segment is then "read," identifying the coarse mask offset. The centroids of all peaks (bars) and symmetric valleys (between evenly-spaced bars) are taken from the projection data via local quadratic fits, then all such centroids are least-squares-fit to their presumed location in the mask template. This linear fit relates the imager coordinates (in pixels) from the captured frame to the coordinate system that was used to generate the barcode; i.e., solve for α and β in the relation:

$$x_{barcode} = \alpha\, x_{pixels} + \beta \qquad (1)$$

where x_{pixels} is a vector of detected feature centroids (in pixels) and $x_{barcode}$ is a vector of the corresponding feature positions in the barcode template (in mm). In addition to the mask offset (β), which is the desired transverse alignment parameter, this technique also produces a scale factor (α) that quantifies the magnification between mask and imager, hence is a function of the longitudinal element spacing. By assuming the center of the imaging array as the local coordinate origin for x_{pixels}, this system is insensitive to scale shifts and mild rotations. The in-plane rotations can also be determined to very high accuracy by using the Hough Transform; measurements [18] have indicated angular resolutions of under 4 arc seconds. Additional details on the barcodes and analysis software are given in Ref. [20].

Performing such a simple analysis on the (x,y) frame projections breaks a complicated 2D cross-correlation operation into two very simple 1D linear fits, enabling the

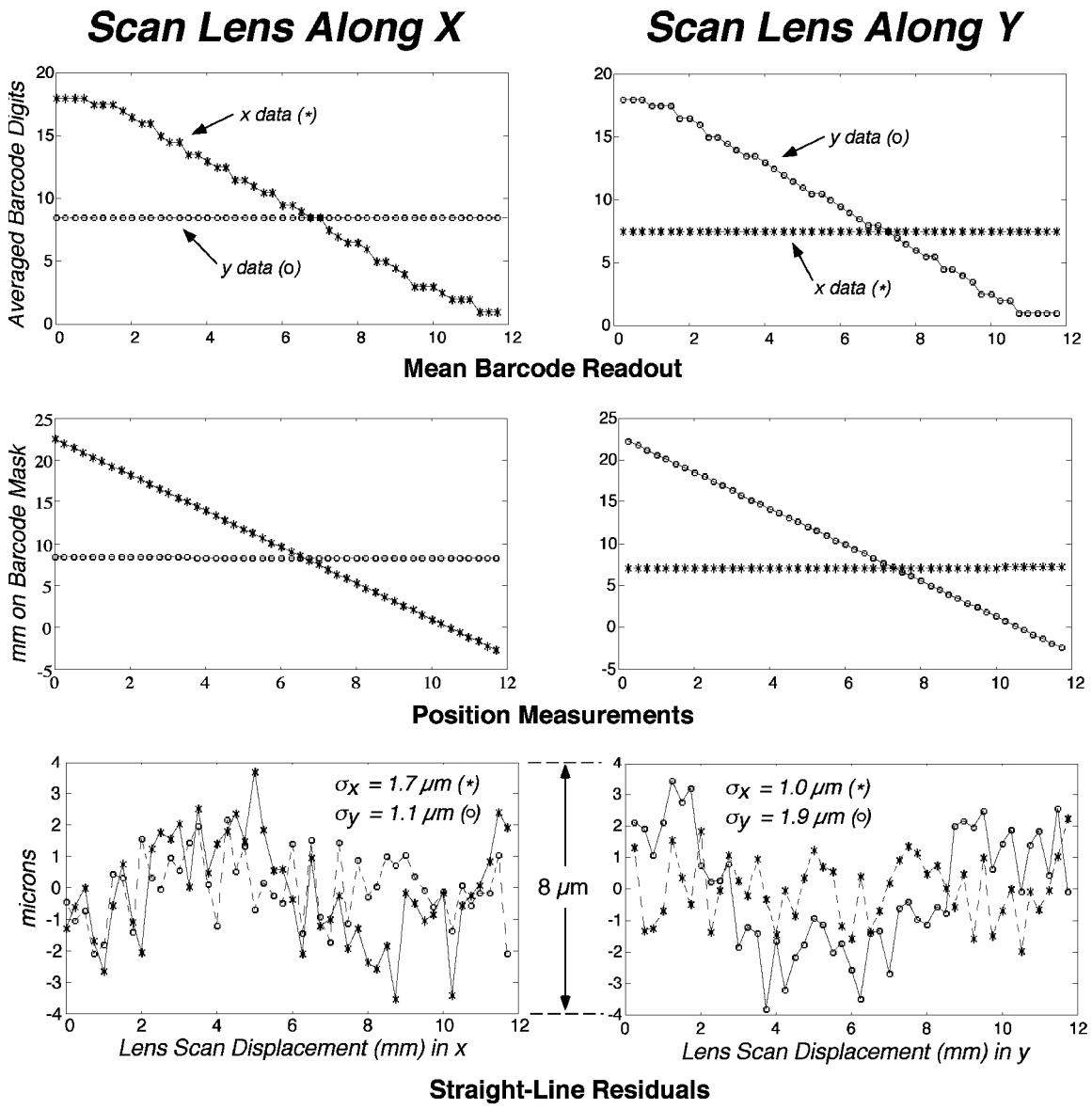

Figure 8: Barcode readings (top), position reconstructions (middle) and straight-line residuals (bottom) for lens scanned 12 mm along x and y axes.

software to execute very quickly, potentially surpassing the 30 Hz frame rate with a simple processor. This analysis procedure has been coded in the MATLAB Version 4.2 interpreter [34], under which the alignment of a frame is calculated in less than a half second on a Power Macintosh 8100/80. By writing the analysis code in a compiled language such as C, one can easily expect a huge gain in speed.

The full 2-dimensional frame can be used to define complicated codes [35] not based on 1-D projections, which can produce enormous measurement range, but also increase the susceptibility to errors and lead to greater processing requirements [36]. The

redundant 2-dimensional barcode of Fig. 6 doesn't deliver nearly as wide a range as possible, but already produces more than enough for most intended implementations, entails a trivial amount of processing overhead, and is quite tolerant of local mask/imager errors, as it spreads its information evenly across the entire frame.

Figure 8 shows test results from a prototype VSM system running across an 8-meter optical baseline with a 2-meter focal length, 42 mm diameter lens used at the midpoint to image the barcode at 1:1 magnification onto a Chinon CX-103 $^1/_3$" video camera. Video data was acquired and averaged via a Data Translation DT2861 frame grabber on an IBM PC (subsequent Macintosh tests have successfully used the SCION LG-3 grabber).

In these tests, the lens was translated, and its position computer-monitored by an Ono-Sokki DF-925 precision digital linear gauge. The horizontal axes of these plots are thus specified in terms of lens displacements; because of the geometry, the equivalent displacements at the source and detector are a factor of two larger.

Data from two scans across the barcode are plotted in Fig. 8. The left column shows the results of a scan across the horizontal (X) axis, and the right column shows the results of a scan across the vertical (Y) axis, as referenced to the barcode drawing in Fig. 6. The top plots show the average between all barcode digits recognized in each frame, which stairsteps down as sequential digits are shifted in and out of the camera's field of view. Since the lens translations are closely aligned with the x and y axes in each respective scan, the scan-orthogonal coordinates are seen to remain quite constant.

The middle plots show the displacement transfer function after the features are fit to the template according to Eq. 1; i.e., lens position, measured in mm, vs. the barcode offset (β) as calculated from the fits (both α and β were free to vary). The factor of two between lens and detector displacement is obvious from these plots. Because the photographic reduction of the barcode mask was not accurately controlled (thus the template scale is not precisely determined), these plots are essentially calibrations, i.e., they relate the coordinates produced by the barcode fit to the physical displacement of alignment system elements (the straight-line sagitta error). The curves are very linear, and span nearly 12 mm of lens displacement (24 mm across the barcode), demonstrating the wide dynamic range needed for application in a large muon detector.

The lower two plots show the deviations in linearity across these scans, projected onto the horizontal (lens position) axes, thus essentially represent the resolution of a straight-line alignment measurement for three equidistant superlayers. The worst-case departures of both x and y residuals remain below 4 μm, and the averaged resolution is

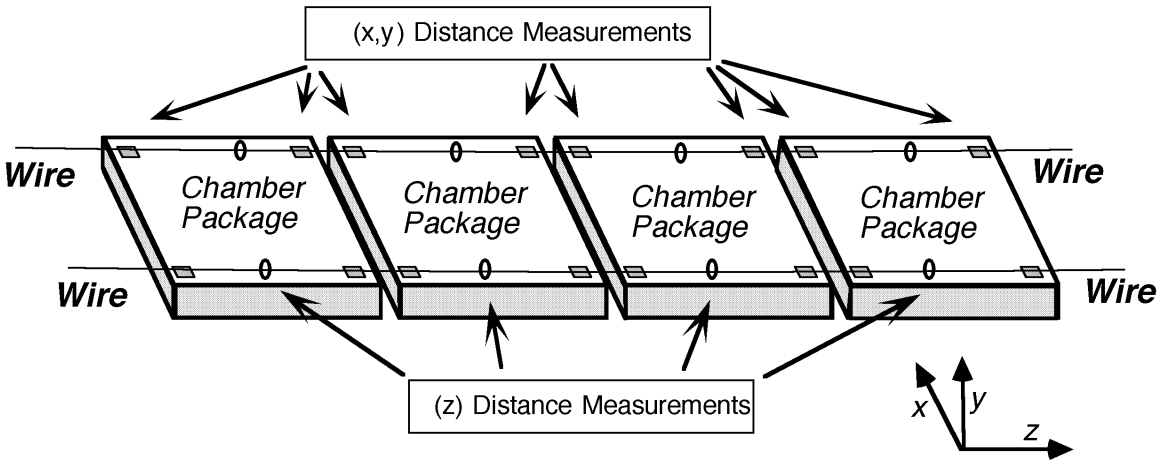

Figure 9: Multipoint, axial alignment across a tiled superlayer with a pair of stretched wires equipped for transverse and axial position readout.

below $\sigma = 2$ μm. These small errors are in large part due to thermally-induced atmospheric disturbances across the 8 meter optical path (these tests took roughly 30 minutes).

Because the VSM is a distributed imaging system, it is relatively insensitive to thermal disturbance near the source and imager. Thermal gradients near the location of the lens have the most impact, as the light ray is effectively back-projected to source and detector in the imaging process, yielding maximum lever arm. Thermal sources at 10° C above ambient temperature have been placed below the lens with limited effects (i.e., below 10 μm shift); thermal and other sensitivities are further examined in Ref. [18].

3) Three-Axis Multipoint Measurements Across a Stretched Wire

Although the 3-point VSM system performs a very precise straight-line alignment measurement, it is difficult to implement in a multipoint fashion, where several alignment measurements are made with reference to a common axis. Adaptations of several VSM's in an overlapping configuration are possible [6,9], but the mechanical complication and expense of such a system can be considerable, and resolution can significantly degrade at the middle of the VSM chain. Other optical multipoint systems are possible using transparent detectors [37] or beamsplitters [38]. These can likewise become quite expensive, and generally exhibit cumulative error from noncoplanarity of the distributed optical surfaces, requiring a potentially complicated calibration.

For this reason, we have pursued concepts that use a stretched wire as a common reference for the in-plane multipoint alignment measurements that relate the component chamber packages within a superlayer, as illustrated in Fig. 9. Inexpensive proximity

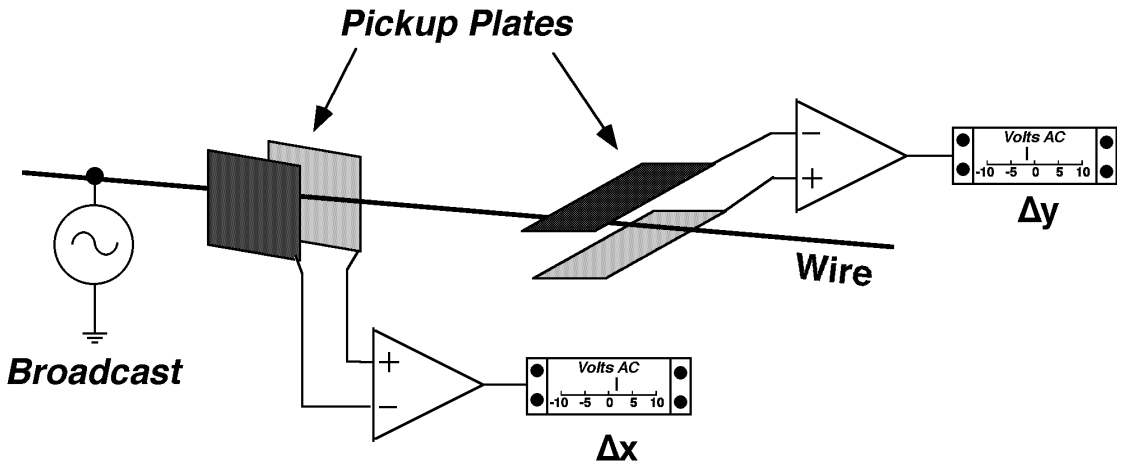

Figure 10: Conventional method of measuring proximity to a stretched wire in a differential capacitor.

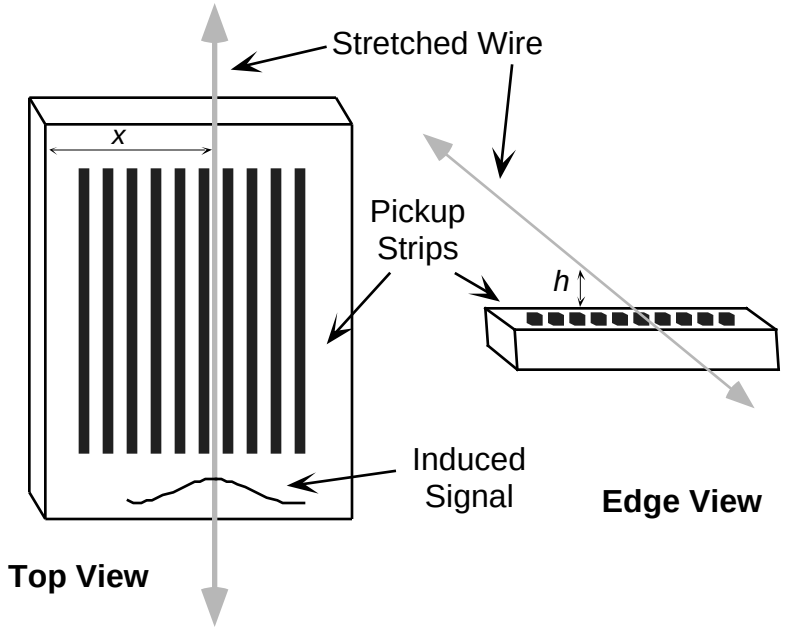

Figure 11: Two-axis (x,h) measurement of wire position with ministrips [39].

pickups can be placed anywhere along the wire (i.e., at the chamber edges and, if required, midway along the perimeter to also monitor chamber deformation), making this a cost-attractive solution. Light, strong, conductively-coated, carbon-composite wires are now becoming available that reduce the sag and vibrational problems traditionally associated with stretched wire alignment [39], and techniques such as measuring the wire's mechanical resonance [40] enable sag to be accurately monitored. Very long stretched wires have been successfully used to align accelerator magnets to very high accuracy [41].

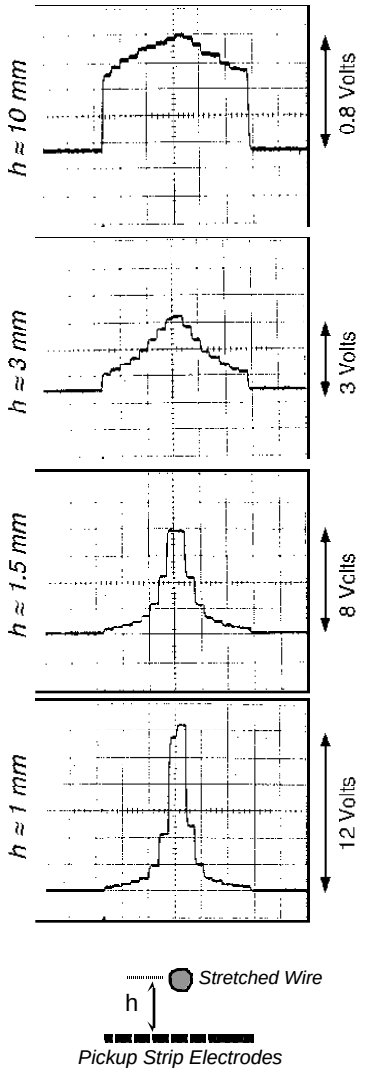

Figure 12: Signal strength from a multiplexed array of 16 adjacent ministrips; the strip number steps along horizontal axis (x) with wire at various heights (h) from strip board.

Fig. 10 depicts the standard method of determining the transverse position of a sensor relative to a conducting wire; i.e., the wire forms a differential capacitor between a set of parallel plates. As the wire approaches one plate or the other, the signal induced from an AC potential on the wire increases on the closer plate (and decreases on the opposite plate), thus the difference between plate signals is a function of wire displacement (the wire position can also be determined optically [42], but this generally has very limited dynamic range or is much more expensive). An accurate measurement across a pair of plates thus relies on very precise electrical and mechanical calibration of the readout components.

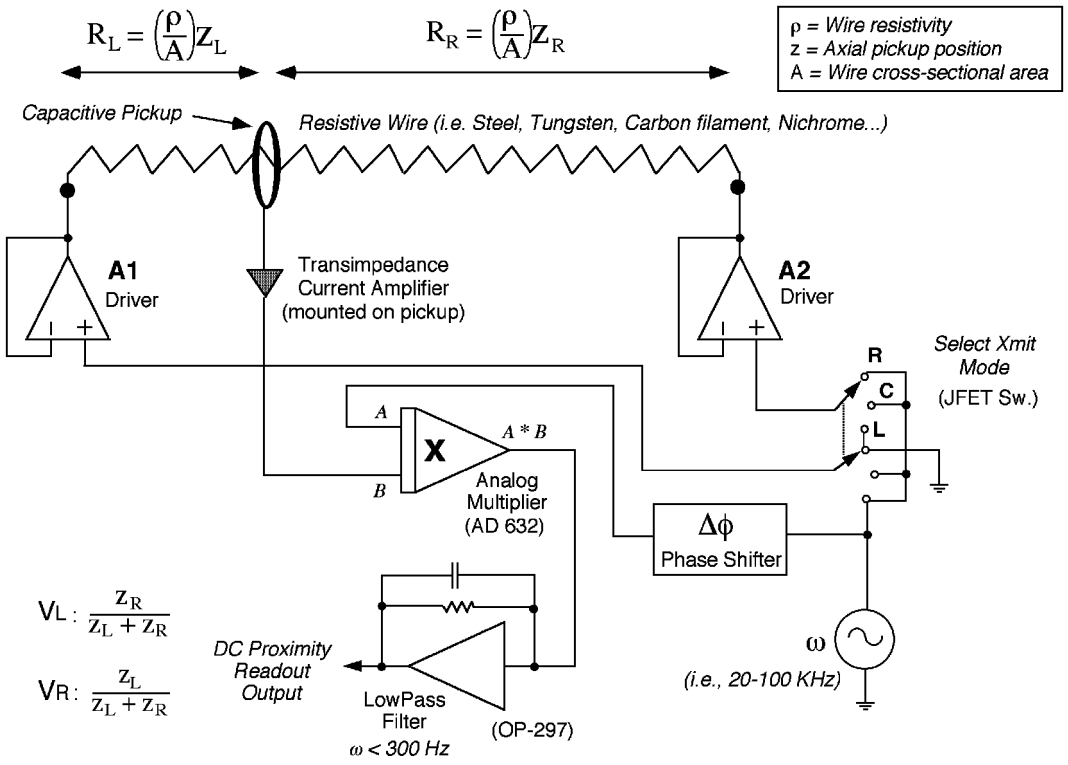

Figure 13: Setup for measuring the axial position along a stretched resistive wire.

An alternative to this conventional scheme, shown in Fig. 11, was proposed and developed by Korytov [39] to relax these requirements, much in the spirit of the RASNIK to VSM evolution described earlier (i.e., the VSM collects many thousands of pixels, vs. the mere 4 channels monitored by the quadrant detector). Here, the pickup electrodes are "pixellated" into a series of strips at a 1 mm pitch; the wire-induced signals on these strips are digitized, allowing the electrostatic footprint of the wire to be effectively "imaged" at the pickup plate, and a precise centroid determined, as indicated in Fig. 12. Since the width and amplitude of the electrostatic image of the wire on the strip plane is strongly correlated with the height of the wire above the strip board (and only weakly correlated with strip board rotation) [7,39], the distance of the wire from the strip plane can also be determined from these measurements, as noted in the data of Fig. 12. For the wire displaced up to 1 cm over the strip board, test results [39] indicated that the wire position could be determined to within $\sigma < 3$ μm across the strips (sagitta direction in Fig. 1) and $\sigma < 100$ μm above the strip board (radial direction in Fig. 1), surpassing the accuracies specified in Section 1 for the axial monitors. A simple electronics scheme based on synchronous detection of a low-frequency RF carrier (20 - 100 kHz) was used to detect and read out the wire signals [10,32,43] at a very modest cost.

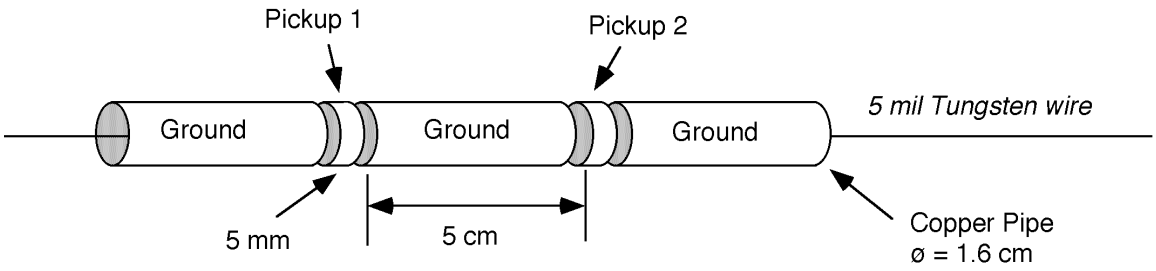

Figure 14: Mechanical layout of the pickup assembly used in axial displacement tests.

Referring to Fig. 9, the mini-strips only measure coordinates in the (x,y) plane normal to the wire. Provided it entails minimal added complexity, a coarser (i.e., mm-level) measurement of the axial coordinate (z) along the wire is also of some interest in the solenoidal detector of Fig. 1. For example, such a measurement can indicate settling and structural deformations during magnet cycling and could be useful during survey and installation.

Fig. 13 shows such a simple method of detecting the axial position of a pickup along a stretched wire. A resistive wire, driven at one end and grounded at the other, is used as a voltage divider, and a shielded cylindrical capacitive pickup performs the function of a contactless potentiometer wiper; i.e., provides a very high impedance (typically, $C < 1$ pf) remote ($r > 1$ cm) tap into the local wire signal. The pickup current is ideally proportional to the driving voltage and capacitive coupling, weighted by the fractional distance along the wire from the location of the pickup to the grounded end. By driving first one end of the wire and grounding the other, then vice-versa (i.e., flipping the switch in Fig. 13 between R and L), and taking the sum over difference of the measured voltages (V_R, V_L), the various gain factors divide out, leaving a clean measurement of the fractional displacement (δ) along the wire, as stated below.

$$\delta \equiv \frac{z_R - z_L}{z_R + z_L} = \frac{V_L - V_R}{V_L + V_R} \tag{2}$$

This technique is similar to that of charge division readout used in drift chambers [44]. Here, however, we can exploit synchronous detection and integrate the signals for a long period, thus achieve a much higher signal-to-noise.

The same wire can be used for the mini-strip readout of transverse and radial coordinates; to obtain maximum signal for this measurement, both ends of the wire would be driven together in phase (with Xmit mode switch in "C" position; Fig. 13), or one end would be left open.

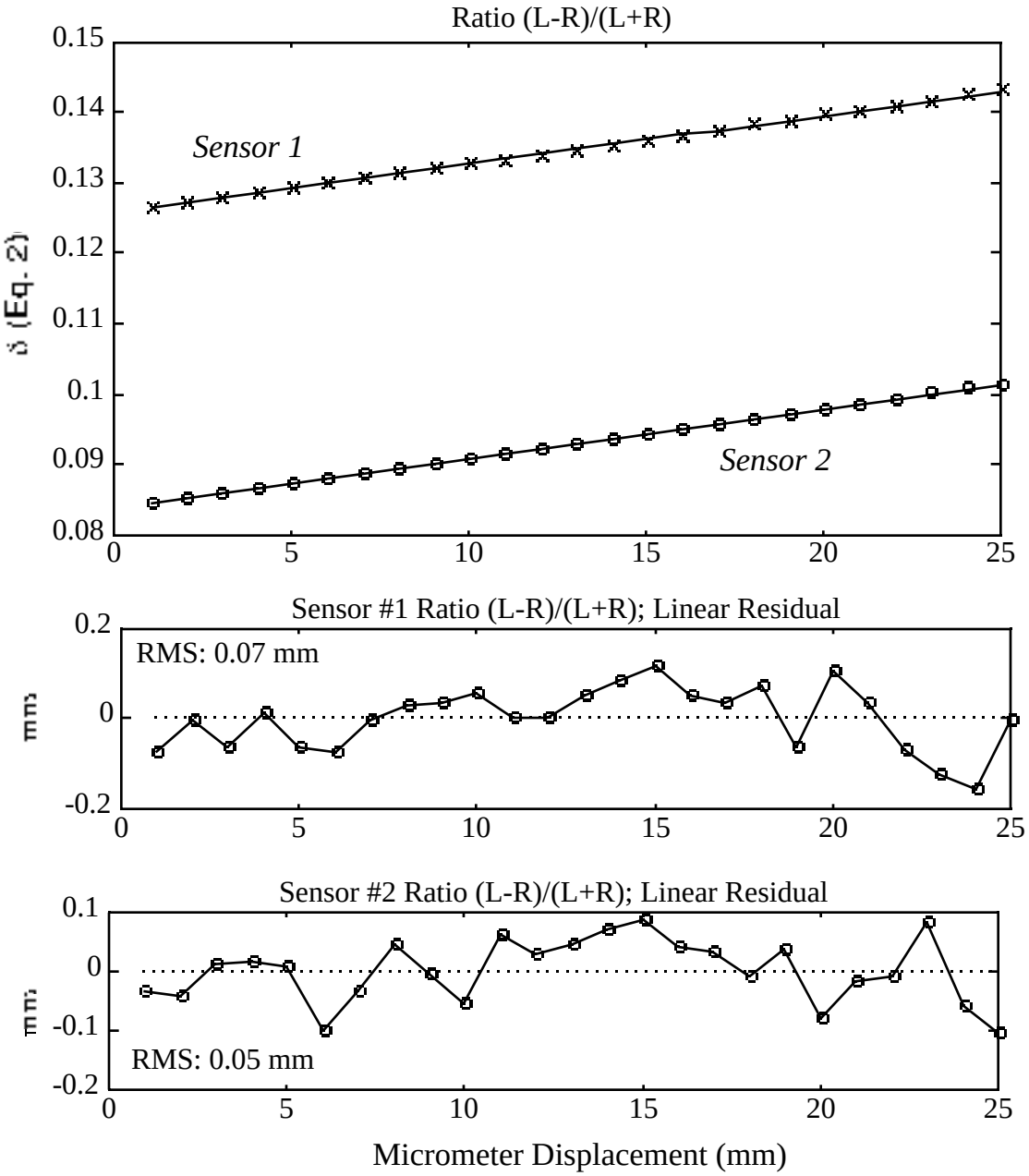

Figure 15: Sum over difference ratio δ and linear residuals for both pickups as a function of local axial displacement across a 3.1 meter span of tungsten wire.

A set of tests have been performed [40] on this system using a simple conducting ring as an axial position pickup. The ring has several advantages as an axial sensor; it presents a large area for efficient coupling into the wire signal, it can be readily shielded such that it is sensitive to a small region of the wire at fixed axial distance, and it is less sensitive to displacement of the wire away from its center [40].

The sensor assembly that was used in the tests is shown in Fig. 13. It is a very simple setup that was fashioned from a standard 1.6 cm inner-diameter copper water pipe. A pair of pickup rings (measuring 5 mm in length) are insulated with fiber washers and sandwiched between a triad of 5-cm grounded segments, which serve to constrain the axial sensitivity of the pickups. Two pickups are built into this unit for cross-checking the consistency of data and calibration; only one is required to make the axial measurement.

Figure 15 shows results from axially scanning the pickup assembly 2.5 cm along a wire, sampling the response of both pickup signals to driving the left and right wire ends after each millimeter of displacement. The pickup sensor assembly was placed near the center of a 3.1 meter long span of 125 μm unplated tungsten wire, driven at each end as shown in Fig. 14. The top plot shows the fractional displacement δ, derived from the measured voltages according to Eq. 2, plotted against micrometer position. The plotted lines are least-squared fits to the data from left (upper) and right (lower) pickups. The data are extremely linear, as supported by the lower plots, which show the residuals of the data points from the fitted line, projected onto the horizontal (position coordinate) axis. The δ ratios are seen to track the micrometer movement to within $\sigma = 70$ μm.

Measurements made with precision translation stages moving the pickup assembly across longer distances (e.g., 1.5 meters [40]) show greater evidence of structured errors caused by imperfections in the wire and defects in the mechanical translator; nonetheless, RMS axial resolutions of under 500 μm were obtained.

When scaling such a measurement up to systems with wires spanning several meters, one must attend to several factors [40] to keep systematic errors low. The nature of the wire is crucial; it should ideally be of uniform resistivity with a low temperature coefficient. The latter factor is addressed by considering a wire made of nichrome ($\Delta\rho/\rho = 0.0002$/°C) or EVENOHM® alloy [45] (used in wirewound resistors; $\Delta\rho/\rho \leq 0.00002$/°C), and the former addressed by using a superior grade of wire or pre-calibrating the wire with an axial scan. Provided a uniform and stable resistive coating can be applied, strong, non-metallic wires (i.e., carbon fiber, silicon carbide [39]) are very well suited to both axial and transverse displacement measurements.

4) Conclusions

A simple system consisting of a miniature video camera, lens, and projected barcode has been shown to work very well as a 3-point straightness monitor, producing 2-axis alignment resolutions of better than $\sigma = 2$ microns over a centimeter of dynamic range and across long optical paths ranging beyond 8 meters in length. A coincident

2-dimensional barcoding scheme allows very efficient image analysis, enabling alignment results to be produced extremely quickly with only modest computation requirements. An inexpensive system for multipoint alignment has also been demonstrated, using a stretched wire with mini-strip pickups for precise transverse measurements and a technique based on charge-division for a coarser, mm-level determination of axial position. As outlined in the proposed implementation of the GEM muon system, these techniques, used together in a hybrid axial/projective arrangement, are able to fulfill the requirements for aligning a large, precision muon detector.

5) Acknowledgments

I'm happy to thank my many colleagues in the former GEM muon team, and especially acknowledge Harry Van der Graaf of NIKHEF Amsterdam, Jacques Govignon of the Draper Laboratory, Andrey Korytov, Louis Osborne, Dale Ross, and Frank Taylor from the Laboratory for Nuclear Science at MIT, Craig Wuest from Lawrence Livermore National Laboratory, and Neil Gershenfeld of the MIT Media Laboratory for many technical discussions. This work was carried out under the GEM muon alignment research and development contracts at the Draper Laboratory in Cambridge, Massachusetts.

6) References

[1] U. Becker, et al., *Nuclear Instruments and Methods*, **A253** (1986), pp. 15-23.
U. Becker, et al., *Nuclear Instruments and Methods*, **A263** (1988), pp. 14-19.
[2] Letter of Intent (LOI) to the Superconducting Super Collider Laboratory by the L★ Collaboration, Chapter 4, November, 1990.
[3] The GEM Collaboration, Technical Design Report, Chapter 4, GEM TN-93-262.
[4] The ATLAS Collaboration, Technical Proposal, CERN/LHCC/94-43, December 15, 1994.
[5] Ostapchuk, A., GEM Note TN-93-334, March 1993.
[6] Paradiso, J., GEM Note TN-92-124, June 1992.
[7] Korytov, A., GEM Note TN-93-302, March 1993.
[8] Mitselmakher, G. and Ostapchuk, A., GEM Note TN-92-202, October 1992.
[9] Paradiso, J., GEM Note TN-92-150, October 1992.
[10] Paradiso, J., GEM Note TN-93-447, August 1993.
[11] Toth, W. E., Draper Laboratory Report CSDL-R-1885, October 1987.
[12] Duinker, P., et al., *Nuc. Inst. and Methods*, A273 (1988), pp. 814-819.

[13] SDC Winerack Group, CDR, Section II-F, SDC Note, SDC-92-179, 1992.
[14] Ayer, F. et al., in Supercollider 4, Plenum Press, New York, 1992, pp. 151-158.
[15] Govignon, J., Ayer, F., SDC Note, SDC-92-393, Dec. 14, 1992.
[16] Govignon, J., Draper Laboratory Report CSDL-R-2598, April 1994.
[17] Post, W., "A Homogeneous Lightsource for RASNIK", NIKHEF-H report, July/August, 1992.
[18] Paradiso, J., GEM Note TN-93-331, May, 1994.
[19] Becker, U. and Paradiso, J., *Nuc. Inst. and Methods*, 196, pp. 381-386 (1982).
[20] Paradiso, J., Goodwin, D., *Proc. of the Third International Workshop on Accelerator Alignment, Annecy, France*, Sept. 28 - Oct. 1, 1993, pp. 131-138.
[21] Dekker, H., et al., *Proc. of the Third International Workshop on Accelerator Alignment, Annecy, France*, Sept. 28 - Oct. 1, 1993, pp. 147-151.
[22] Marshall Electronics Inc., Culver City, California, USA.
Supercircuits Inc., Leander, Texas, USA, *http://www.scx.com.*
Surveillance Sound Products Inc., Hauppage, New York, USA.
[23] Paradiso, J., GEM Note TN-94-608, June 1994.
[24] Fletcher, P., *Electronic Design*, Vol. 41, No. 12, June 10, 1993, pp. 29-32.
[25] Muirhead, I., *Laser Focus World*, Vol. 32, No. 12, December 1996, pp. 87-90.
[26] *Circuit Cellar INK*, No. 58, May 1995, p. 9.
[27] *MacUser*, Vol. 11, No. 4, April 1995, p. 69.
[28] Griswold, M.A., MRI Unit, Beth Israel Hospital, Boston, Massachusetts, USA, Personal communication, May 1996.
[29] Aebi, V.W., et al., "Radiation Hardened Stellar Sensor Final Report," EO Sensors Division , Intevac, Inc., Palo Alto, CA, Report No. BMO-TR-94-04, May 1993.
[30] Bencze, G. and Brunel, L., CMS Collaboration, CERN, Personal communication, September 1996.
[31] Wentink, R., Carbone, J., *Nuclear Instruments and Methods in Physics Research*, **A347**, pp. 522-528, 1994.
Downing, R.G., Zeissler, C.J., and Chen, H., SPIE Conference Proceedings Vol. **1737**, 1992, pp. 308-321.
Zarnowski, J., et al., "Radiation Tolerant CID Imager," Technical Report, CID Technologies Inc., Liverpool NY, 1994.
[32] Paradiso, J., Marlow, D., *Proc. of the 1994 LeCroy Electronics for Future Colliders Conference*, LeCroy Corp., Chestnut Ridge, NY, May 1993, pp. 235-249.
[33] Heckel, W., Optical 3-D Measurement Techniques II, Herbert Wichmann Verlag GmbH, Karlsruhe, Germany, 1993, pp. 125-132.

Ge, R., *ibid.*, pp. 239-246.
[34] The Math Works, Inc., Cochituate Place, 24 Prime Parkway, Natick, MA. 01760.
[35] The ATLAS Collaboration, Muon Note 113, June 1995.
[36] Hashemi, K.S. and Bensinger, J.R., ATLAS Muon Note 92, August 1995.
[37] Blum, W., et al., *Nuclear Instruments and Methods in Physics Research,* **A367**, pp. 413-417, 1995.
[38] Gayde, J.C., Lasseur, C., CMS Collaboration Document TN/94-250, August 1994.
[39] Korytov, A., Osborne, L., Paradiso, J., Rosenson, L. and Taylor, F., *Nuclear Instruments and Methods in Physics Research,* **A343**, pp. 428-434, 1994.
[40] Paradiso, J., GEM Note TN-94-607, May 1994.
[41] Coosemans, W., *Proc. of the Third International Workshop on Accelerator Alignment, Annecy, France,* Sept. 28 - Oct. 1, 1993, pp. 223-240.
Ruland, R.E., et al., *ibid.*, pp. 241-252.
Wilson, I., CERN SL/92-41.
[42] Sawicki, R., Bliss, E., Griffith, L., in GEM Note TN-93-339, March 1992.
[43] Paradiso, J., Gershenfeld, N., *Computer Music Journal,* Vol. 21, Spring 1997.
[44] Radeka, V. and Rehak, P., *IEEE Transactions on Nuclear Science,* Vol. NS-25, February 1978, pp. 46-52.
[45] Carpenter Technology Corporation, Carpenter Steel Division, Caldwell, New Jersey, USA, datasheet for EVANOHM® Alloy R.